Targeting PBR by Hexaminolevulinate-Mediated Photodynamic Therapy Induces Apoptosis through Translocation of Apoptosis-Inducing Factor in Human Leukemia Cells

Ingegerd Eggen Furre,[1] Susan Shahzidi,[1] Zivile Luksiene,[2] Michael T.N. Møller,[1] Elin Borgen,[1] Janet Morgan,[3] Kinga Tkacz-Stachowska,[1] Jahn M. Nesland,[1] and Qian Peng[1,4]

[1]Department of Pathology, The Norwegian Radium Hospital, University of Oslo, Oslo, Norway; [2]Institute of Material Sciences and Applied Research, Vilnius University, Vilnius, Lithuania; [3]Department of Dermatology, Roswell Park Cancer Institute, Buffalo, New York; and [4]State Key Laboratory for Advanced Photonic Materials and Devices, Fudan University, Shanghai, China

Abstract

Photodynamic therapy (PDT) with endogenous protoporphyrin IX derived from 5-aminolevulinic acid or its derivatives has been established for treatments of several premalignancies and malignancies; however, the mechanism of the modality is not fully elucidated. The mitochondrial permeability transition pore consists mainly of the mitochondrial outer membrane voltage-dependent anion channel and the peripheral benzodiazepine receptor (PBR) and the mitochondrial inner membrane adenine nucleotide translocator (ANT). These mitochondrial proteins are responsible for the permeability transition that leads to apoptosis. In the present study, the human leukemia cell line, Reh, was treated with PDT using hexaminolevulinate (HAL). More than 80% of apoptotic Reh cells were found after HAL-mediated PDT (HAL-PDT) with high-molecular-weight (50 kbp) DNA fragmentation. Addition of PK11195 or Ro5-4864, two ligands of PBR, during HAL-PDT significantly inhibited the apoptotic effect. Bongkrekic acid, a ligand for ANT, also reduced the PDT effect. Although the mitochondrial transmembrane potential collapsed, neither cytosolic translocation of mitochondrial cytochrome *c* nor activation of caspase-9, caspase-8, caspase-3, and poly(ADP-ribose) polymerase were found. However, nuclear translocation of mitochondrial apoptosis-inducing factor (AIF) was shown by both immunoblotting and immunocytochemistry. Because AIF is the sole one among all proapoptotic factors involved in caspase-dependent and caspase-independent pathways that induces the high-molecular-weight DNA fragmentation, we conclude that HAL-PDT specifically targets PBR, leading to apoptosis of the Reh cells through nuclear translocation of mitochondrial AIF. This study suggests PBR as a possible novel therapeutic target for HAL-based PDT of cancer. (Cancer Res 2005; 65(23): 11051-60)

Introduction

Heme biosynthesis occurs partially inside and partially outside of the mitochondria, starting in the cytosol with the condensation of two molecules of 5-aminolevulinic acid to porphobilinogen followed by the condensation of four porphobilinogen molecules to uroporphyrinogen III by porphobilinogen deaminase. Coproporphyrinogen III is formed from the decarboxylations of uroporphyrinogen III and translocated through the outer mitochondrial membrane. In the intermembrane space of the mitochondria, coproporphyrinogen III is oxidized to protoporphyrinogen IX and later to protoporphyrin IX (PpIX) at the inner mitochondrial membrane. Heme biosynthesis is complete with the incorporation of iron into PpIX by ferrochelatase. By adding exogenous 5-aminolevulinic acid or its derivatives, the naturally occurring porphyrins, PpIX in particular, may selectively accumulate in some tumors because of a high activity of porphobilinogen deaminase with a concomitant low activity of ferrochelatase (1, 2). Such selectivity has been exploited in photodynamic therapy (PDT), a modality that involves systemic or topical administration of a tumor-localizing photosensitizer (or prodrug) and its subsequent activation by visible light to result primarily in singlet oxygen–induced photodamage to the tumor (1–3).

Although PDT with 5-aminolevulinic acid or its derivatives has been established for routine clinical treatments of several superficial cutaneous premalignancies and malignancies, the exact mechanisms responsible for killing diseased cells are still not fully elucidated. Apoptosis, or cell suicide, is a form of cell death that is distinct from necrosis. The morphologic characteristics of the apoptotic cells include cell shrinkage, plasma membrane blebbing, chromatin condensation, and nuclear fragmentation. Eventually, the cells break into small apoptotic bodies with membrane-surrounded fragments, which are cleared by phagocytosis without inciting an inflammatory response. Apoptosis can be induced by diverse stimuli, including PDT in many tumor cells *in vitro* and *in vivo* (3–7).

Two distinct benzodiazepine receptors have been identified: one is restricted to brain and is called central benzodiazepine receptor and the other is present in most peripheral tissues, such as adrenals, kidney, and the hematopoietic system, and is called the peripheral benzodiazepine receptor (PBR; ref. 8). The PBR is an 18 kDa receptor protein and is localized to outer mitochondrial membrane. It is physically associated with the 32 kDa voltage-dependent anion channel (VDAC), an outer membrane protein, and the 30 kDa adenine nucleotide translocator (ANT), an inner membrane protein. VDAC and ANT constitute the backbone of the mitochondrial permeability transition pore, a multiprotein complex that is located at the contact site between inner and outer mitochondrial membranes. The permeability transition pore is intimately involved in the initiation and regulation of apoptosis by

Note: Supplementary data for this article are available at Cancer Research Online (http://cancerres.aacrjournals.org/).

Requests for reprints: Qian Peng, Department of Pathology, The Norwegian Radium Hospital, University of Oslo, Montebello, 0310 Oslo, Norway. Phone: 47-22935553; Fax: 47-22934832; E-mail: qian.peng@labmed.uio.no.

doi:10.1158/0008-5472.CAN-05-0510

controlling mitochondrial membrane potential and releasing proapoptotic factors from the mitochondria (9).

PBR has a high-affinity recognition site for porphyrins, PpIX in particular, and uses the porphyrins as endogenous ligands (10–12). As the synthesis of PpIX takes place within the mitochondria, PpIX and its precursors must traverse the inner and outer mitochondrial membranes. The mechanism of this transport is not known; however, one possibility is that after initially binding to the PBR, the transport occurs as a result of an interaction between ANT and VDAC.

The reaction of singlet oxygen ($^1O_2$) with biomolecules is generally regarded as the principal initiating pathway leading to photodynamic damage. Because $^1O_2$ diffuses intracellularly <0.02 μm in its lifetime (13) and because endogenously synthesized PpIX, being a ligand for PBR, is formed in the mitochondria and transported through the permeability transition pore, then components of the pore close to a high concentration of PpIX and $^1O_2$ are expected to be the primary targets of PDT when 5-aminolevulinic acid or its derivatives are used. The damaged permeability transition pore may trigger apoptotic processes by disruption of the mitochondrial transmembrane potential ($\Delta\Psi_m$) and releases of mitochondrial proapoptotic factors.

The aim of the present study was to investigate the mechanism of apoptotic induction by PDT with hexaminolevulinate (HAL, a hexylester of 5-aminolevulinic acid shown to be 50-100 times more efficient at inducing formation of PpIX than 5-aminolevulinic acid itself; ref. 14) in a human non-T, non-B lymphoblastic leukemia cell line (Reh). We found that HAL-based PDT targeted PBR and led to an apoptosis-inducing factor (AIF)–dependent pathway of apoptosis in the Reh cells.

Materials and Methods

Chemicals. HAL was kindly provided by PhotoCure ASA (Oslo, Norway). It was freshly dissolved for each experiment, initially in a small amount of ethanol (with a final concentration of <1%) followed by dilution in serum-free RPMI 1640 (Life Technologies, Gaithersburg, MD). A stock solution of exogenous PpIX (Sigma, St. Louis, MO) was prepared in 1 N perchloric acid/methanol (1:1, v/v) and kept at −70°C. PK11195 and Ro5-4864 were initially dissolved in DMSO and were diluted in medium with a final concentration of DMSO <1%. All other chemicals used were of the highest purity available.

Cell cultivation. The human non-T, non-B lymphoblastic leukemia cell line Reh was grown in RPMI 1640 (Life Technologies) containing 10% fetal bovine serum (FBS), 100 units/mL penicillin, and 100 μg/mL streptomycin (Biowhittaker, Walkersville, MD) in a fully humidified incubator (US Autoflow, Nuaire, Plymouth, MN) at 37°C with 5% CO_2. The cells were subcultured thrice a week to a density of 2×10^5 cells/mL to keep them in an exponential growth phase. Cell density was kept constant for all experiments at 8×10^5 cells/mL because our initial studies showed that HAL-mediated PpIX production is cell density dependent.

Subcellular localization of hexaminolevulinate-induced protoporphyrin IX. Cells were seeded in six-well tissue culture plates and then incubated with serum-free RPMI 1640 containing either 5 or 25 μmol/L of HAL for 3.5 hours followed by adding 500 nmol/L of a fluorescent mitochondrial probe, MitoTracker Green FM (Molecular Probes, Eugene, OR) for 30 minutes. After being washed once with PBS containing 5% FBS, the cells were transferred to glass slides and a cover glass was gently put on the top. The subcellular localization patterns of both HAL-induced PpIX and MitoTracker were studied by fluorescence microscopy (Nikon Eclipse E800, Nikon, Tokyo, Japan) with a 100 W halogen lamp. Fluorescent images were made by a highly light sensitive thermoelectrically cooled charge-coupled device camera ($ORCA_{II}$-ER, Hamamatsu, Japan). The filter combinations used were composed of a 380 to 420 nm excitation filter, a 430 nm beam splitter, and a 630 ± 20 nm emission filter for PpIX; and a 465 to 495 nm excitation filter, a 505 beam splitter, and a 515 to 555 nm emission filter for MitoTracker. A neutral density filter (ND16) was used to reduce photobleaching of PpIX fluorescence.

Photodynamic treatment with hexaminolevulinate. Cells were seeded into dishes (Nunclon) and incubated in the dark for 4 hours in RPMI 1640 containing 5 μmol/L of HAL but without serum to avoid porphyrin excretion to the culture medium. The cells were then exposed to light from a bank of four fluorescent tubes (model 3026, Applied Photophysics, London, United Kingdom) emitting light mainly around 450 nm. The irradiance was kept constant for all experiments at 8 mW/cm^2. The medium was removed immediately after irradiation and replaced with HAL-free RPMI 1640 containing 10% FBS. In separate experiments, cells were incubated with the serum-free medium containing exogenous PpIX (0.5 μmol/L) for 4 hours and then irradiated with the same light source at a dose of 160 mJ/cm^2.

Cell viability assay. Cell viability was assessed with a commercially available kit using a colorimetric method based on the cellular conversion of a tetrazolium compound, 3-(4,5-dimethylthiazol-2-yl)-5-(3-carboxymethoxyphenyl)-2-(4-sulfophenyl)-2*H*-tetrazolium, inner salt (MTS; Promega, Madison, WI), into a colored formazan product. This product can be quantitatively measured by 492 nm absorbance and is directly proportional to the number of living cells in the culture. Treated cells (8×10^4) were diluted in RPMI 1640 to a final volume of 100 μL in wells of a 96-well microplate and 20 μL of MTS (5 mg/mL) was then added to the wells to incubate for 1.5 hours at 37°C. The absorbance at 492 nm was measured 20 hours after HAL-mediated PDT (HAL-PDT) with a microplate reader (Labsystems Oy, Helsinki, Finland). The absorbance of blank wells containing medium and MTS but no cells was subtracted from all experimental readings, and cell survival is expressed as the fraction of control samples. In some experiments, cell growth was assessed by directly counting numbers of living cells under a phase-contrast microscope without prior staining at various times after HAL-PDT with PK11195 or Ro5-4864.

Morphologic studies of apoptosis. Apoptotic cells were identified by fluorescence microscopy based on nuclear morphology after staining cells with 4 μg/mL Hoechst 33342 (Sigma) at 37°C for 30 minutes. For quantification, at least 200 cells of each sample were counted and the percentage of apoptotic cells was calculated. Each experiment was done in triplicate. For the experiments with exogenous PpIX, the cells were double stained with Hoechst 33342 for the detection of living and apoptotic cells and with propidium iodide (2 μg/mL at 37°C for 5 minutes) for necrotic cells. For electron microscopy, control and PDT-treated cells were prepared as described before (15).

DNA electrophoresis. DNA from control and PDT-treated cells were isolated according to the instructions of Apoptotic DNA ladder kits (Life Technologies). Equivalent amounts of DNA were subjected to electrophoresis on 2% agarose gel for the 100 bp DNA ladder kit (75 V for 1.5 hours) and on 0.4% agarose gel for the high-molecular-weight DNA kit (25 V for 18 hours) at room temperature. Finally, DNA fragmentation was visualized by ethidium bromide staining. Positive controls (in the kits) and molecular weight DNA markers were included.

Effects of hexaminolevulinate-mediated photodynamic therapy on the permeability transition pore. To directly image the PBR and to study the specificity of the PBR ligand PK11195 for the Reh cell line, a specific fluorescent probe for the PBR, FGIN-1-27 (Alexis Biochemicals, San Diego, CA; ref. 16), was used. Cells were incubated with FGIN-1-27 (0.5 μmol/L) for 45 minutes in the absence and presence of PK11195 (200 μmol/L; Sigma) to determine if PK11195 could inhibit binding of the fluorescent probe to PBR. For PDT treatment, PK11195 or Ro5-4864 (a PBR ligand; Sigma) at concentrations of 5 to 20 μmol/L was added to cells during incubation with HAL, and cell growth was examined at various times after light by counting the number of living cells. In separate experiments, the apoptotic cells were counted by fluorescence microscopy at 4 and 20 hours after HAL-PDT plus PK11195. The effects of bongkrekic acid (Calbiochem, San Diego, CA), a ligand for ANT that inhibits permeability transition, were also examined in the study. Cell survival was determined by the MTS assay after the cells had been treated with HAL-PDT in the presence of bongkrekic acid (50 μmol/L, initially dissolved in 2 N NH_4OH and added during HAL incubation).

Mitochondrial transmembrane potential. Mitochondrial transmembrane potential ($\Delta\Psi_m$) was studied using a $\Delta\psi_m$-sensitive fluorescent probe, JC-1 (5,5′,6,6′ -tetrachloro-1,1′,3,3′-tetraethylbenzidazolcarbocyanin iodide; Biotium, Inc., Hayward, CA). At different time intervals after PDT, cells were collected and incubated with the JC-1 solution (1:100 dilution) for 10 minutes before being analyzed by a FACSCalibur flow cytometer (Becton Dickinson, San Jose, CA) with an argon laser (488 nm) for the excitation and FL1 at 520 to 540 nm and FL2 at 575 to 595 nm for the emission detection. In some experiments, the cells were also stained with Hoechst 33342 for an additional 5 minutes and examined by the same fluorescence microscopy as described previously. The filter combinations used were composed of a 330 to 380 nm excitation filter, a 400 nm beam splitter, and a 420 nm emission filter for Hoechst 33342; and a 540 ± 20 nm excitation filter, a 565 nm beam splitter, and a 605 ± 55 nm emission filter for JC-1.

Caspase activity. The activities of caspase-9 and caspase-3 were measured with colorimetric assay kits (Chemicon, Temecula, CA). Cells at various times after PDT were collected and suspended in lysis buffer for 10 minutes at 0°C. Lysates were centrifuged to precipitate cellular debris. The amounts of proteins in the lysates were determined. Lysate proteins (150 μg) from each sample were incubated for 3 hours at 37°C in reaction buffer containing caspase-9 substrate (Ac-LEHD-pNA) or caspase-3 substrate [*N*-acetyl-Asp-Glu-Val-Asp (DEVD)-*p*-nitroanilide] according to the instructions of the manufacturer. Absorbance at 405 nm was read on a microtiter plate reader. The specificity of each enzyme activity was verified by using the corresponding specific caspase inhibitors provided by the supplier. A human breast cancer cell line (MA-11) shown to specifically activate procaspase-3 after treatment with an immunotoxin was included as a positive control (17). Furthermore, HAL-PDT was carried out with 100 μmol/L of the potent, cell-permeable, and irreversible inhibitor (Ac-DEVD-CMK; Calbiochem) of caspase-3, caspase-6, caspase-7, caspase-8, and caspase-10 according to the instructions of the manufacturer, and percentages of apoptotic cells were counted.

Subcellular fractionation and Western blot analysis. Subcellular fractionation (cytosolic versus mitochondrial/nuclear) of samples was prepared according to the method described by Strømhaug et al. (18). In brief, the cells were electrodisrupted by a single high-voltage pulse in 500 μL ice-cold sucrose (10%), followed by homogenization on ice to disrupt 95% of the cells. The resulting homogenates were centrifuged at 50,000 × *g* for 30 minutes. Supernatants (cytosolic fraction) were transferred to fresh tubes and kept at −70°C until analysis. The pellets (mostly mitochondrial and nuclear fractions) were resuspended in 0.5 mL of lysis buffer [20 mmol/L Tris-HCl (pH 7.2), 5 mmol/L EDTA, 5 mmol/L EGTA, 10 mmol/L sodium PPi, and 0.4% SDS] and sonicated for 15 seconds. The protein, ANT, was used as a marker for the mitochondrial fraction (data not shown). In some experiments, whole-cell samples were also included and lysed in the same procedure. Proteins in the fractionated and whole-cell extracts were quantified by the Bradford method (19) using the bicinchoninic acid protein assay kit (Pierce, Inc., Rockford, IL). Equal amounts of proteins from cytosolic and mitochondrial/nuclear fractions were electrophoresed on SDS-polyacrylamide gel (12-15%), the gel-separated proteins were transferred to polyvinylidene difluoride membranes, and the membranes were probed overnight at 4°C with primary antibodies. Each of the targeted proteins was immunostained by up to five distinct antibodies from at least two different sources to verify data. The antibodies presented were as follows: anti-PBR and anti-AIF (both rabbit; Santa Cruz Biotechnology, Santa Cruz, CA); anti–cytochrome *c* and anti-caspase-8 [both mouse; BD Biosciences (Franklin Lakes, NJ) and Cell Signalling Technology (Beverly, MA), respectively]; and anti-Bid/tBid, anti-cleaved caspase-9, anti-cleaved caspase-3, and anti-poly(ADP-ribose) polymerase (anti-PARP; all rabbit; Cell Signalling Technology). After probing, the membranes were washed thrice and then incubated for 1 hour at room temperature with the respective anti-rabbit/mouse horseradish peroxidase–conjugated secondary antibodies (diluted 1:2,000) before visualization by using a chemiluminescence detection kit (Amersham Biosciences, Piscataway, NJ).

Immunocytochemistry of apoptosis-inducing factor. Before and after PDT, cells were collected and washed with PBS containing 1% FBS. After fixation with methanol followed by washing thrice with the same PBS, the cells were transferred to glass slides by cytospin and dried overnight at room temperature. The cells were permeabilized with 0.1% saponin in PBS for 10 minutes, incubated with rabbit anti-AIF primary antibody (1:25 dilution; Santa Cruz Biotechnology) for 90 minutes at room temperature, and subsequently incubated with Alexa Fluor 488 donkey anti-rabbit secondary antibody (1:200 dilution; Molecular Probes) for 45 minutes at room temperature. Finally, nuclei were stained with Vectashield mounting medium containing 4′,6-diamidino-2-phenylindole (DAPI, Vector Laboratories, Burlingame, CA). The slides were viewed by fluorescence microscopy.

Statistical analysis. The two-tailed Student's *t* test was used to analyze differences between PDT alone and PDT plus PK11195, Ro5-4864, bongkrekic acid, or caspase-3 inhibitor. Data are presented as mean values ± SD. All tests were done at the 0.05 significance level.

Results

Subcellular localization of hexaminolevulinate-induced protoporphyrin IX and its photodynamic therapy effect. The intracellular colocalization pattern of HAL-mediated endogenous PpIX and a mitochondrial probe, MitoTracker, in the Reh cells was studied by fluorescence microscopy (Fig. 1*A*). Because the fluorescence signal of endogenous PpIX induced by the therapeutic dose of 5 μmol/L of HAL was weak and photobleached fast under the microscopic light, a higher but nontoxic concentration of 25 μmol/L of HAL was applied for the acquisition of the fluorescence images. The granular patterns and distribution of fluorescence in the extranuclear fraction of the cells were similar for both PpIX and the mitochondrially localizing MitoTracker, indicating that the HAL-induced PpIX was primarily confined to the mitochondria of the Reh cells. Additionally, some weak PpIX fluorescence was seen in the plasma and nuclear membranes but not in the nuclear region. This is probably due to diffusion of PpIX from the mitochondria.

As shown in Fig. 1*B*, pretreatment of cells with 5 μmol/L of HAL led to a dose-dependent response of cell survival to light exposure, whereas cells exposed to light only or HAL alone had little effect on cell survival. A 50% decrease in cellular viability, as measured by the MTS assay, was produced at 20 hours after HAL-PDT with a light dose of 160 mJ/cm^2 (Fig. 1*B*). This PDT dose was chosen for the rest of this study.

Hexaminolevulinate-mediated photodynamic therapy induces apoptotic death in Reh cells. The induction of apoptosis by PDT was assessed by characteristic morphologic and biochemical criteria. Initially, the apoptotic cells were identified by fluorescence microscopy using Hoechst 33342 for nuclear staining. The time course studies showed typical apoptotic cells with cellular shrinkage and peripheral chromatin condensation starting from 4 hours after PDT (Fig. 2*A*). The percentage of apoptotic cells increased with time after PDT with >80% apoptotic cells at 20 hours (Fig. 2*B*). The discrepancy between the cell viability (Fig. 1*B*) and percentage of apoptotic cells following PDT may be because the MTS assay for cell viability is based on activities of dehydrogenase enzymes in metabolically active cells and some apoptotic cells may still retain the activities of such enzymes. Fluorescence microscopy might also overestimate the percentage of apoptotic cells by including some secondary necrotic cells. Electron microscopy analysis of PDT-treated cells showed characteristic morphology of apoptotic alterations with chromatin condensation and fragmentation and the formation of apoptotic bodies (Fig. 2*C*). These indications of apoptosis were accompanied by 50 kbp high-molecular-weight

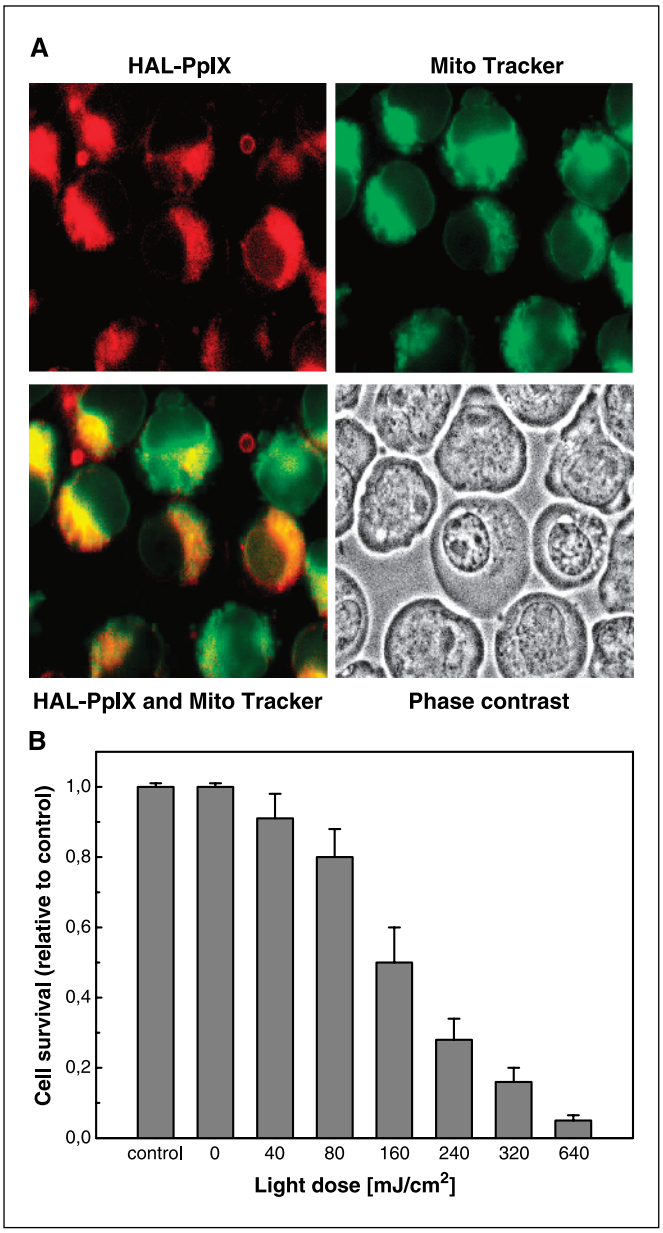

Figure 1. Subcellular localization of HAL-induced endogenous PpIX and its phototoxicity of the Reh cells. *A,* fluorescence and corresponding phase-contrast images of HAL-induced PpIX (*red*), MitoTracker (*green*), and PpIX/MitoTracker (*red/green superimposition*) in the Reh cells incubated with 25 μmol/L HAL for 4 hours and MitoTracker (500 nmol/L) for 30 minutes. *B,* light dose–dependent phototoxicity of the Reh cells preincubated with 5 μmol/L HAL for 4 hours followed by light exposure. Cell survival was examined by MTS assay.

DNA fragmentation, a typical DNA fragmentation induced by AIF, as early as 1 hour after PDT (Fig. 2*D*). No oligonucleosomal DNA fragmentation was found at any time studied following PDT (data not shown). Interestingly, when cells were treated with PDT using 0.5 μmol/L of exogenous PpIX, only necrotic cells could be detected by both fluorescence and electron microscopy at 1 to 20 hours after treatment (Fig. 2*E*). This indicates that PDT with exogenous PpIX does not induce apoptosis in the Reh cells.

Involvement of the permeability transition pore in hexaminolevulinate-mediated photodynamic therapy–induced apoptosis. The PBR, for which PpIX is a ligand, may be a target of PDT with HAL-induced PpIX. However, no change in the PBR levels was detected by Western immunoblotting at any time point after PDT (Fig. 3*A*), suggesting that HAL-PDT does not affect PBR expression. Before PK11195 and Ro5-4864, two well-known ligands for the PBR, were used to investigate the involvement of the PBR in PDT-induced apoptosis, the specificity of PK11195 for the PBR in this particular Reh cell line had been determined by displacement of the fluorescent PBR ligand FGIN-1-27. When the cells were incubated with FGIN-1-27 alone, fluorescence was seen in the cytoplasm of the cells. Incubation of the cells with FGIN-1-27 in the presence of PK11195 resulted in the disappearance of the fluorescence (data not shown), indicating that PK11195 completely inhibits the binding of FGIN-1-27 to the PBR. Addition of PK11195 or Ro5-4864 at increasing concentrations during HAL-PDT gave rise to a dose-dependent increase in cell survival (Fig. 3*B*), whereas treatments with ligands alone (without PDT) showed no effect on the cell growth (data not shown). At 24 hours after treatment, the numbers of cells were increased from 16% and 11% (PDT alone) of controls to 78% and 91% (PDT plus 20 μmol/L of PK11195 or Ro5-4864; $P = 0.005$ for PK11195 and $P = 0.005$ for Ro5-4864), respectively, demonstrating that these two PBR ligands can efficiently inhibit the effect of HAL-PDT on the cell growth. Furthermore, only 12% and 13% of apoptotic cells were determined by microscopy at 4 and 20 hours, respectively, after PDT with PK11195 (20 μmol/L) in comparison with 36% and 80% of apoptosis induced by PDT alone (data not shown), clearly indicating that the PBR is involved in the apoptotic induction by HAL-PDT. Because ANT, an inner membrane protein of the mitochondria, may be associated with PpIX transportation from the mitochondria to the cytosol, it may be another target of HAL-PDT. Bongkrekic acid, a ligand for the ANT, significantly suppressed the effect of HAL-PDT on cell death ($P = 0.036$; Fig. 3*C*), suggesting that the ANT is also involved in the apoptotic cell death induced by PDT.

Mitochondrial transmembrane potential. Disruption of $\Delta\psi_m$ is one of the early events in induction of apoptosis. A $\Delta\psi_m$-sensitive dye, JC-1, was used to examine whether loss of $\Delta\psi_m$ is associated with HAL-PDT–induced apoptosis. JC-1 accumulates in the mitochondria with a transmembrane potential, forming aggregates marked by punctate orange-red fluorescence. When the electrochemical gradient across the mitochondrial membrane collapses in apoptotic cells, the reagent does not accumulate in the mitochondria and no aggregates form. As early as 1 hour after HAL-PDT, $\Delta\psi_m$ loss was already seen in 40% of the cells (Fig. 3*D*), although morphologic evidence of apoptosis was not yet observed (data not shown). At later stages following PDT, the percentages of the cells losing $\Delta\psi_m$ were increased up to 82% at 20 hours (Fig. 3*D*). Figure 3*E* shows fluorescence and phase-contrast images of the treated cells costained with JC-1 and Hoechst 33342 at 20 hours after PDT. Consistently, undamaged cells show normal morphology with bright red punctuated fluorescence typical of a normal $\Delta\Psi_m$, whereas some neighboring cells show characteristic apoptotic morphology with green fluorescence, indicating the loss of $\Delta\psi_m$.

Hexaminolevulinate-mediated photodynamic therapy–induced apoptosis is cytochrome *c* independent. The mitochondria-initiated pathway of caspase-activating cascades is the most characterized pathway for regulation of apoptosis. It involves cytosolic translocation of mitochondrial cytochrome *c* that activates caspase-9 and further the downstream effector, caspase-3. Western blotting of subcellular fractionated samples shows that cytochrome *c* is

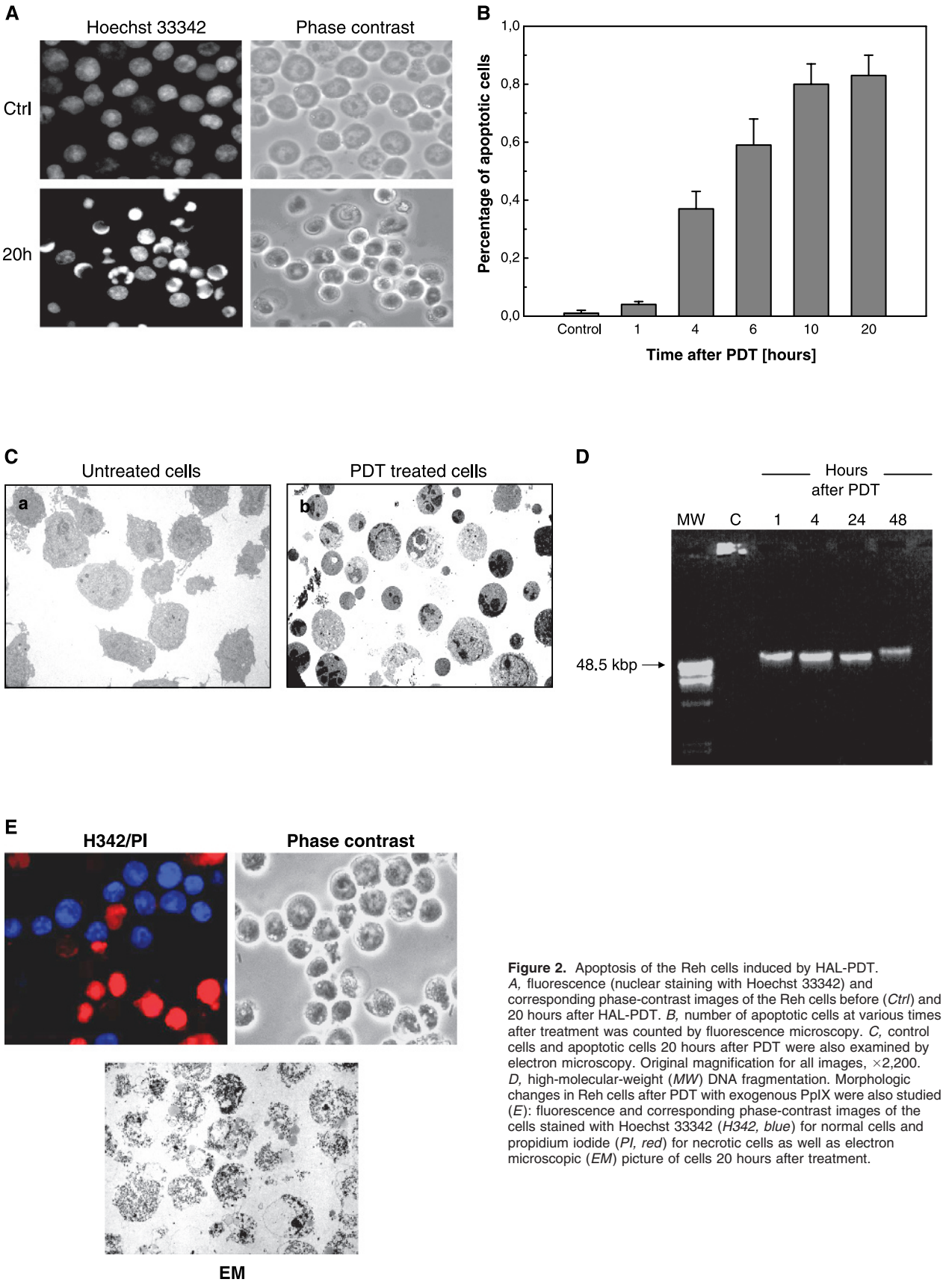

Figure 2. Apoptosis of the Reh cells induced by HAL-PDT. *A,* fluorescence (nuclear staining with Hoechst 33342) and corresponding phase-contrast images of the Reh cells before (*Ctrl*) and 20 hours after HAL-PDT. *B,* number of apoptotic cells at various times after treatment was counted by fluorescence microscopy. *C,* control cells and apoptotic cells 20 hours after PDT were also examined by electron microscopy. Original magnification for all images, ×2,200. *D,* high-molecular-weight (*MW*) DNA fragmentation. Morphologic changes in Reh cells after PDT with exogenous PpIX were also studied (*E*): fluorescence and corresponding phase-contrast images of the cells stained with Hoechst 33342 (*H342, blue*) for normal cells and propidium iodide (*PI, red*) for necrotic cells as well as electron microscopic (*EM*) picture of cells 20 hours after treatment.

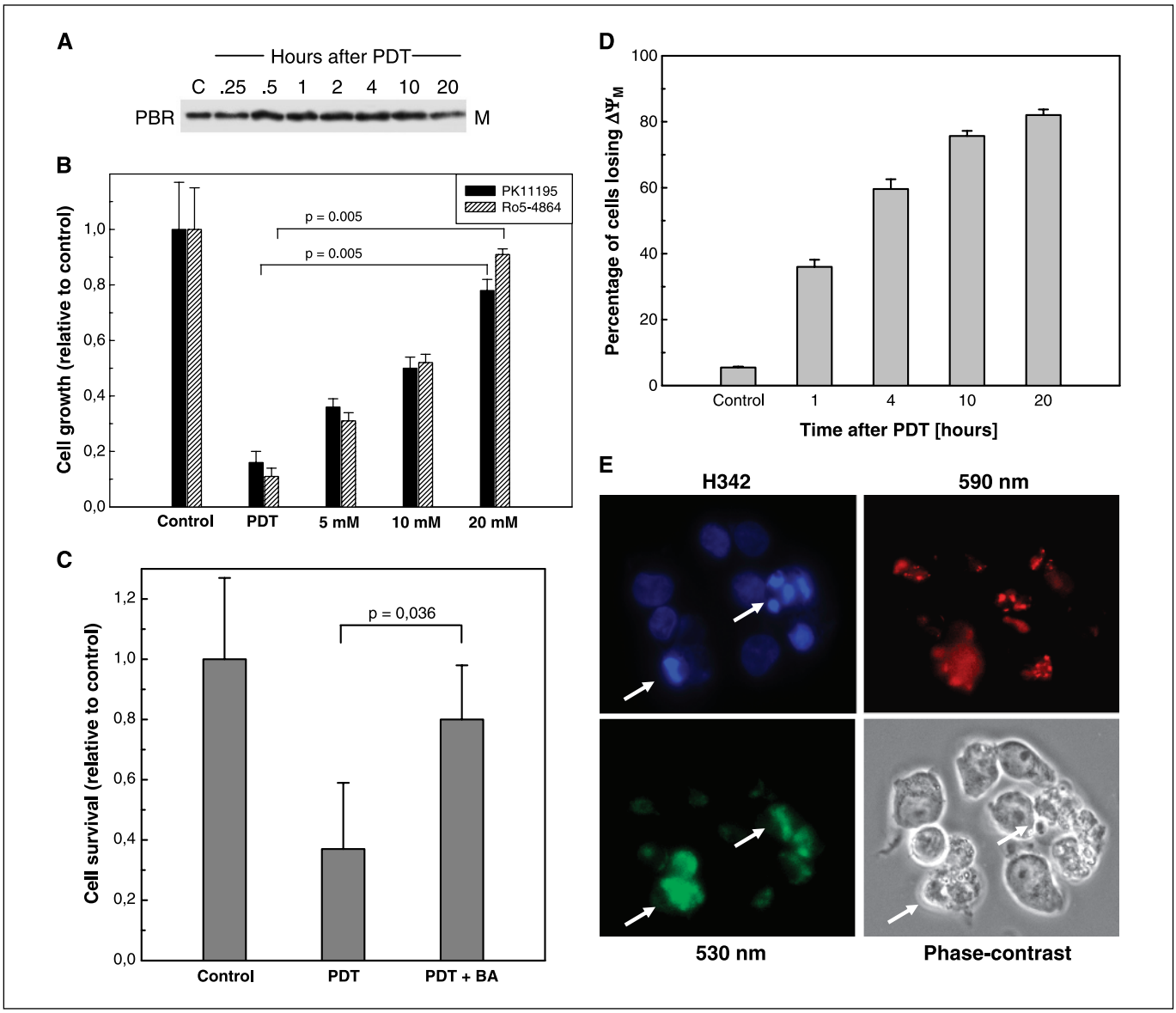

Figure 3. Involvement of the permeability transition pore in HAL-PDT–induced apoptosis. *A,* Western blotting of PBR in the mitochondrial/nuclear fraction of cells at various times after HAL-PDT by using an antibody against PBR. *B,* cell growth as a function of concentrations of PK11195 and Ro5-4864 applied during HAL-PDT as measured by microscopically counting the numbers of cells. *C,* effect of bongkrekic acid (*BA*, 50 μmol/L) on cell survival 20 hours after HAL-PDT, as determined by MTS assay. *D,* percentages of the cells with the loss of $\Delta\psi_m$ at various times after HAL-PDT was determined by flow cytometry with the $\Delta\psi_m$ indicator JC-1. Based on at least three different samples. *Columns,* percentage of the cells losing $\Delta\psi_m$; *bars,* SD. *E,* fluorescence and corresponding phase-contrast images of the cells costained with JC-1 and Hoechst 33342 (*blue*) 20 hours after HAL-PDT. *Red fluorescence* (590 nm), $\Delta\psi_m$ in undamaged cells; *green fluorescence* (530 nm), apoptotic cells. The images of Hoechst 33342 are also included.

present in the mitochondrial/nuclear fraction, whereas almost no cytochrome *c* can be seen in the cytosolic fraction. The levels of cytochrome *c* in the mitochondrial/nuclear fractions are constant at various times after PDT (Fig. 4*A*). Five anti–cytochrome *c* antibodies from different suppliers were used with the same finding, showing clearly that cytochrome *c* was not released from the mitochondria of the cells after PDT. Furthermore, the upstream caspase-8 was not cleaved and Bid was not truncated (Fig. 4*A*). In addition, no cleavage of the downstream caspase-9, caspase-3, and PARP was observed by immunoblotting (Fig. 4*B*). The activities of caspase-9 and caspase-3 were also measured with no significant change after PDT (Fig. 4*C*). Finally, apoptotic cells were quantified after PDT in the presence or absence of a potent inhibitor of caspase-3, caspase-6, caspase-7, caspase-8, and caspase-10, and no significant difference in apoptotic induction was found ($P = 0.37$; Fig. 4*D*). These results show that mitochondria-initiated and perhaps also cell surface death receptor-induced pathways of caspase-activating cascades are not involved in the induction of apoptosis by HAL-PDT.

Hexaminolevulinate-mediated photodynamic therapy–induced apoptosis involves nuclear translocation of mitochondrial apoptosis-inducing factor. AIF is a mitochondrial protein that translocates from the mitochondria initially, to the cytosol, and then to the nucleus where it induces caspase-independent apoptosis with typical high-molecular-weight (50 kbp) DNA fragmentation. Figure 5*A* shows that, by Western

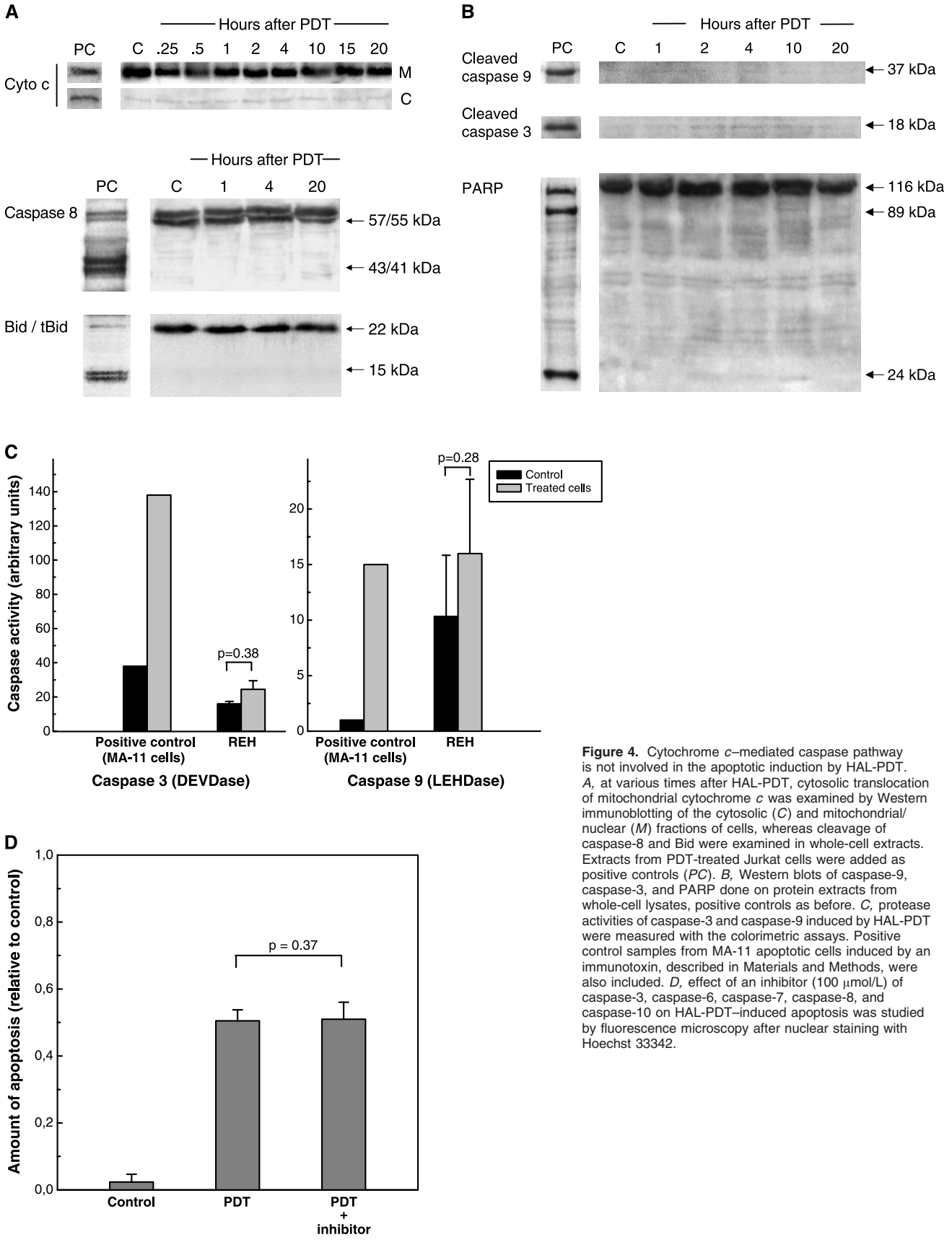

Figure 4. Cytochrome *c*–mediated caspase pathway is not involved in the apoptotic induction by HAL-PDT. *A,* at various times after HAL-PDT, cytosolic translocation of mitochondrial cytochrome *c* was examined by Western immunoblotting of the cytosolic (*C*) and mitochondrial/nuclear (*M*) fractions of cells, whereas cleavage of caspase-8 and Bid were examined in whole-cell extracts. Extracts from PDT-treated Jurkat cells were added as positive controls (*PC*). *B,* Western blots of caspase-9, caspase-3, and PARP done on protein extracts from whole-cell lysates, positive controls as before. *C,* protease activities of caspase-3 and caspase-9 induced by HAL-PDT were measured with the colorimetric assays. Positive control samples from MA-11 apoptotic cells induced by an immunotoxin, described in Materials and Methods, were also included. *D,* effect of an inhibitor (100 μmol/L) of caspase-3, caspase-6, caspase-7, caspase-8, and caspase-10 on HAL-PDT–induced apoptosis was studied by fluorescence microscopy after nuclear staining with Hoechst 33342.

blotting, AIF is present only in the mitochondrial/nuclear fraction of control cells. However, it appears in the cytosolic fraction from 30 minutes to 10 hours after PDT, with concurrent decreases in the amount of AIF in the mitochondrial/nuclear fraction, and then decreases in the cytoplasm at 15 and 20 hours after PDT with an increase in the mitochondrial/nuclear fraction. The results suggest that there is translocation of AIF from the mitochondria to the cytosol and further to the nucleus. With immunocytochemistry, AIF exhibited a granular pattern in the extranuclear fraction of control cells (Fig. 5*B*), indicating its normal mitochondrial localization. At 20 hours after PDT treatment, AIF showed a diffuse pattern in the cytoplasm and some in the nuclear regions (Fig. 5*B*), confirming the results of immunoblotting. These findings, together with high-molecular-weight DNA fragmentation, convincingly show that the event of nuclear translocation of mitochondrial AIF is involved in the induction of apoptosis by HAL-PDT in the cells.

Discussion

Although the concept of apoptosis was introduced more than three decades ago (4), the mechanisms of how apoptosis is initiated and executed are still not completely understood. During the past decade, tremendous progress has been made in understanding apoptosis partly as a result of molecular identification of the mitochondrial permeability transition pore. Recently, the key components of the pore, particularly PBR, have been proposed as molecular targets for anticancer chemotherapy (20) as well as for PDT (21, 22).

The present study has shown that HAL-induced endogenous PpIX mainly localized in the mitochondria of the Reh cells (Fig. 1*A*). After light exposure, >80% of the cells died by apoptosis (Fig. 2*A* and *B*). The apoptotic induction by HAL-PDT was both light dose dependent (Fig. 1*B*) and time course dependent (Fig. 2*B*). The apoptosis was further confirmed by electron microscopy, which enables to distinguish morphologically apoptosis from necrosis (Fig. 2*C*; ref. 23). DNA electrophoreses exhibited only high-molecular-weight (50 kbp) DNA fragmentation (Fig. 2*D*), the typical size of fragmented DNA seen in AIF-induced apoptosis (24). However, when cells were treated with PDT using 0.5 μmol/L of exogenous PpIX, a concentration approximating to the amount of endogenous PpIX theoretically produced by 5 μmol/L of HAL, no apoptotic cells were found; however, necrotic cells were found (Fig. 2*E*), suggesting that different mechanisms were involved.

Although the molecular properties of the mitochondrial permeability transition pore have not been fully characterized yet, the core components of permeability transition pore are considered to be VDAC and PBR in the mitochondrial outer membrane and ANT in the mitochondrial inner membrane. These mitochondrial proteins cooperate to form a large conductance channel that spans both the inner and outer mitochondrial membranes. In its open state, this channel facilitates the transport of adenine nucleotides and other anions between the mitochondrial matrix and the cytoplasm. Porphyrins, in particular PpIX, are well known as ligands of the PBR (10–12). In the heme biosynthetic pathway, although coproporphyrinogen III may traverse the channel from the cytosol to the matrix (25–28), the HAL-induced endogenous PpIX may also use this channel for its transportation from the matrix to the cytosol (25–27). Because the targets of PDT are the sites where the photosensitizer is localized, any sensitive biological structures associated with porphyrin transportation channel at the inner and outer mitochondrial membranes are among the targets for PDT with endogenous PpIX induced by HAL.

Displacement of the specific fluorescent PBR ligand, FGIN-1-27, by PK11195 in the present study showed the specificity of PK11195 for the PBR in the Reh cell line. Both PK11195 and Ro5-4864 significantly inhibited the HAL-PDT–induced apoptosis, suggesting that PBR is a major target of HAL-PDT and is involved in the induction of apoptosis. Moreover, bongkrekic acid, which binds to ANT and helps maintain the permeability transition pore in its closed configuration (29), significantly suppressed the effect of HAL-PDT on apoptotic cell death (Fig. 3*C*), indicating that ANT may be another target of HAL-PDT. There may be a relationship between PBR and ANT as targets because of their physically close association (30), their proximity to HAL-induced endogenous PpIX synthesis at the mitochondrial inner membrane, and the possibility that PpIX may use ANT for its transportation. Thus, effects on one of the two proteins targeted by PDT may influence the other. These results are supported by the finding with exogenous PpIX, which was unable to induce apoptosis after light exposure. Exogenous PpIX localizes intracellularly differently than endogenous PpIX and may not target the PBR sufficiently to produce the same degree of apoptosis. Kessel et al. (31) compared PpIII, PpXIII, and PpIX and

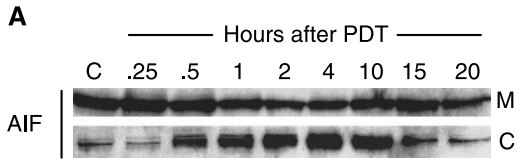

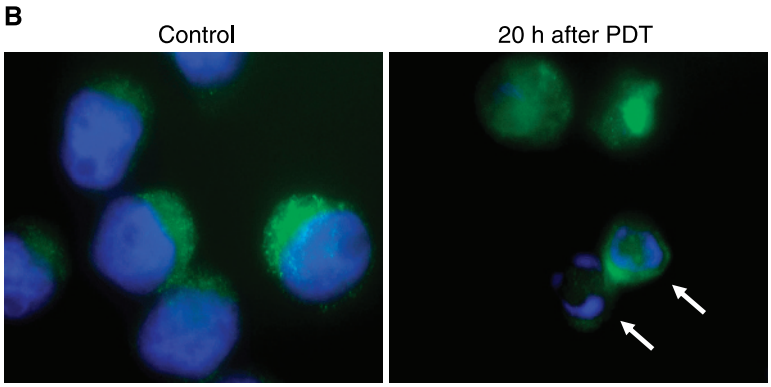

Figure 5. AIF-induced, caspase-independent pathway is involved in the apoptotic induction of apoptosis by HAL-PDT. *A,* nuclear translocation of mitochondrial AIF was examined by Western immunoblotting of the cytosolic and mitochondrial/nuclear fractions of cells at various times after HAL-PDT. *B,* immunocytochemistry of AIF in the cells before (*control*) and 20 hours after HAL-PDT. *Green fluorescence,* AIF; *blue fluorescence* (DAPI), nuclei.

found that all three agents could induce 30% to 40% apoptotic cells after light exposure, although only PpIX had a high affinity for PBR. However, addition of PK11195 or Ro5-4864 had no effect on phototoxicity, indicating that the apoptosis induced by PDT with exogenous PpIX probably occurred through a mechanism independent of PBR.

The $\Delta\Psi_m$ results from the asymmetrical distribution of protons and ions on both sides of the inner mitochondrial membrane. This leads to chemical (pH) and electric gradients that are essential for mitochondrial function. Normally, $\Delta\Psi_m$ is regulated tightly by the passage of ions and molecules. The dissipation of $\Delta\Psi_m$ is an early event of the apoptotic cascade. Disruption of the permeability transition pore that regulates the potential of the inner mitochondrial membrane is responsible for the preapoptotic $\Delta\Psi_m$ collapse. Permeability transition can permit depolarization of the membrane as a result of changes in redox state, pH, etc. Bongkrekic acid and cyclosporin A are well-known ligands for ANT, which suppress the preapoptotic $\Delta\Psi_m$ disruption and thus inhibit apoptosis, indicating a role for the permeability transition in apoptosis. In agreement with these data, we found that the mitochondrial membrane potential was disrupted as early as 1 hour after HAL-PDT. Further, bongkrekic acid could almost abolish the PDT effect (Fig. 3*C*), suggesting the involvement of ANT in HAL-PDT–induced dissipation of $\Delta\Psi_m$. A similar finding was reported with a porphyrin-like photosensitizer, verteporfin (32).

Opening of the permeability transition pore as well as rapid $\Delta\Psi_m$ disruption as a result of specifically targeting the PBR and perhaps also the ANT by HAL-PDT may lead to the release of mitochondrial proapoptotic factors, such as cytochrome *c* and AIF. Once released into the cytosol, these mitochondrial proteins respectively mediate a caspase-dependent apoptotic pathway or translocate further into the nucleus to induce a caspase-independent apoptotic pathway (24). In the present study, both pathways with cytochrome *c* and AIF were investigated.

Cytochrome *c* normally resides exclusively in the intermembrane space of the mitochondria, whereas apoptotic protease activating factor-1 (Apaf-1) and procaspase-9 are cytosolic proteins. After cytosolic translocation, cytochrome *c* works with Apaf-1 and procaspase-9 in the presence of dATP (the complex is called the apoptosome) to initiate apoptotic process by activating the downstream effector caspase-3. Neither release of cytochrome *c* nor cleavage of the upstream caspase-8 as well as Bid and of the downstream caspase-9 and caspase-3 was seen in this study (Fig. 4*A* and *B*). This is consistent with the results that show no change in the activities of caspase-9 and caspase-3 after PDT (Fig. 4*C*). Furthermore, cleavage of a cellular target of caspase-3, PARP, a downstream event in apoptosis, was not observed (Fig. 4*B*). In addition, Ac-DEVD-CMK, an inhibitor of caspase-3 as well as of caspase-6, caspase-7, caspase-8, and caspase-10, did not alter the effect of HAL-PDT on apoptotic induction. These data indicate that both mitochondria-initiated and perhaps also cell surface death receptor–mediated, caspase-dependent pathways are not involved in the induction of apoptosis by HAL-PDT in the Reh cells.

AIF is a nuclear-encoded protein that translocates from the mitochondrial intermembrane space into the cytosol and further to the nucleus where it induces a caspase-independent peripheral chromatin condensation with high-molecular-weight (50 kbp) DNA fragmentation (24). This is in agreement with our finding (Fig. 2*D*) in the present study. By Western blot analyses of fractionated cell samples, we found that AIF moved from the mitochondrial/nuclear fraction into the cytosolic fraction during a period of 0.5 to 10 hours after HAL-PDT, followed by its reappearance in the mitochondrial/nuclear fraction (Fig. 5*A*), indicating nuclear translocation of AIF from the mitochondria. This finding was further confirmed by immunocytochemistry (Fig. 5*B*). Similar results were also found in human T-cell lymphoma cell line (Jurkat) and colon carcinoma cell lines (Colon205 and HCC2998) after HAL-PDT (see Supplementary Data). Apoptosis is characterized by either high-molecular-weight (50 kbp) DNA fragmentation or internucleosomal (200 bp) DNA fragmentation, depending on the apoptosis inducers. The evidence of nuclear translocation of mitochondrial AIF obtained from the present study does not necessarily indicate that AIF is solely involved in the apoptotic induction by HAL-PDT. However, because among all proapoptotic factors involved in mitochondria-initiated caspase-dependent (cytochrome *c*, Smac/DIABLO, and HtrA2/OMI) and caspase-independent (AIF and endonuclease G; ref. 33) and nonmitochondria-induced caspase-dependent (cell surface death receptor) pathways, AIF is the only one that has been shown to induce the high-molecular-weight DNA fragmentation thus far, the results of this study show that the apoptotic induction by HAL-PDT is AIF-dependent.

Currently, it is not known how the opening of the permeability transition pore at the inner membrane leads to loss of outer membrane integrity; however, one theory is that disruption of $\Delta\Psi_m$ results in swelling of the mitochondrial matrix, mechanical rupture of the outer membrane, and release of intermembrane proteins, such as cytochrome *c* and AIF (34). The finding by Daugas et al. (35) that dissipation of $\Delta\Psi_m$ occurs concurrently with nuclear translocation of mitochondrial AIF indicates a correlation between $\Delta\Psi_m$ disruption and AIF translocation. This can be prevented by permeability transition inhibitors, such as bongkrekic acid and cyclosporin A (36). Thus, it seems that the loss of $\Delta\Psi_m$ is responsible for the AIF translocation, whereas the release of cytochrome *c* is not strictly dependent on $\Delta\Psi_m$ (37–39). Recent studies have suggested that the components of the permeability transition pore work together with proteins of Bcl-2 family to control the permeability transition pore opening in a specific manner for the release of mitochondrial proapoptotic proteins (39–42). Two sites that help control the permeability transition pore have been proposed, the S and the P sites (40–42). The S site, which is cyclosporin A or bongkrekic acid sensitive (41), is responsible for the release of AIF, whereas the P site, which is cyclosporine A insensitive, is involved in the release of cytochrome *c*. $^1O_2$, produced in most cases of PDT, has been shown to be associated with the S site (41). These observations are in good agreement with our results in the present study, suggesting that $^1O_2$ produced by HAL-PDT damages and/or modulates specifically the PBR and perhaps also the ANT, facilitating the opening of the permeability transition pore for the AIF release via effects on the S site, which, in turn, induces apoptosis of the Reh cells.

Acknowledgments

Received 2/15/2005; revised 8/29/2005; accepted 9/19/2005.

The costs of publication of this article were defrayed in part by the payment of page charges. This article must therefore be hereby marked *advertisement* in accordance with 18 U.S.C. Section 1734 solely to indicate this fact.

We thank Elisabeth Emilsen, Ellen Hellesylt, and Maria Rypdal for excellent technical assistance; Dr. Yvonne Andersson (Department of Tumor Biology, The Norwegian Radium Hospital, University of Oslo, Oslo, Norway) for providing apoptotic MA-11 cells; and PhotoCure ASA for HAL.

References

1. Peng Q, Berg K, Moan J, Kongshaug M, Nesland JM. Review: 5-aminolevulinic acid-based photodynamic therapy: principle and experimental research. Photochem Photobiol 1997;65:235–51.
2. Peng Q, Warloe T, Berg K, et al. Review: 5-aminolevulinic acid-based photodynamic therapy: clinical research and future challenges. Cancer 1997;79:2282–308.
3. Dougherty TJ, Gomer CJ, Henderson BW, et al. Review: photodynamic therapy. J Natl Cancer Inst 1998; 90:889–905.
4. Kerr JRF, Wyllie AH, Currie AR. Apoptosis: a basic biological phenomenon with wide-ranging implications in tissue kinetics. Br J Cancer 1972;26:239–57.
5. Wyllie AH. The biology of cell death in tumors. Anticancer Res 1985;5:131–6.
6. Fisher DE. Apoptosis in cancer therapy: crossing the threshold. Cell 1994;78:539–42.
7. Agarwal ML, Clay ME, Harvey EJ, Evanes HH, Antunez AR, Oleinick NL. Photodynamic therapy induces rapid cell death by apoptosis in L5178Y mouse lymphoma cells. Cancer Res 1991;51:5993–6.
8. Braestrup C, Squires RF. Specific benzodiazepine receptors in rat brain characterized by high-affinity [^{3}H]diazepam binding. Proc Natl Acad Sci U S A 1977;74: 3805–9.
9. Ly JD, Grubb DR, Lawen A. The mitochondrial membrane potential ($\Delta\Psi_m$) in apoptosis; an update. Apoptosis 2003;8:115–28.
10. Verma A, Nye JS, Snyder SH. Porphyrins are endogenous ligands for the mitochondrial (peripheral-type) benzodiazepine receptor. Proc Natl Acad Sci U S A 1987;84:2256–60.
11. Snyder SH, Verma A, Trifiletti RR. The peripheral-type benzodiazepine receptor: a protein of mitochondrial outer membranes utilizing porphyrins as endogenous ligands. FASEB J 1987;1:282–8.
12. Pastorino JG, Simbula G, Gilfor E, Hoek JB, Farber JL. Protoporphyrin IX, an endogenous ligand of the peripheral benzodiazepine receptor, potentiates induction of the mitochondrial permeability transition and the killing if cultured hepatocytes by rotenone. J Biol Chem 1994;269:31041–6.
13. Moan J, Berg K. The photodegradation of porphyrins in cells can be used to estimate the lifetime of singlet oxygen. Photochem Photobiol 1991;53:549–53.
14. Gaullier JM, Berg K, Peng Q, et al. Use of 5-aminolevulinic acid esters to improve photodynamic therapy on cells in culture. Cancer Res 1997;57:1481–6.
15. Peng Q, Warloe T, Moan J, et al. Antitumor effects of 5-aminolevulinic acid-mediated photodynamic therapy can be enhanced by the use of a low dose of Photofrin in human tumor xenografts. Cancer Res 2001; 61:5824–32.
16. Kozikowski AP, Kotoula M, Ma D, Boujrad N, Tuckmantel W, Papadopoulos V. Synthesis and biology of 7-nitro-2,1,3-benzoxadiazol-4-yl derivative of 2-phenylindole-3-acetamide: a fluorescent probe for the peripheral-type benzodiazepine receptor. J Med Chem 1997;40:2435–9.
17. Andersson Y, Juell S, Fodstad Ø. Downregulation of the antiapoptotic MCL-1 protein and apoptosis in MA-11 breast cancer cells induced by an anti-epidermal growth factor receptor-*Pseudomonas* exotoxin a immunotoxin. Int J Cancer 2004;112:475–83.
18. Strømhaug PE, Berg TO, Fengsrud M, Seglen PO. Purification and characterization of autophagosomes from rat hepatocytes. Biochem J 1998;335:217–24.
19. Bradford MM. A rapid and sensitive method for quantitation of microgram quantities of protein utilizing the principle of protein-dye binding. Anal Biochem 1976;72:248–54.
20. Costantini P, Jacotot E, Decaudin D, Kroemer G. Mitochondrion as a novel target of anticancer chemotherapy. J Natl Cancer Inst 2000;92:1042–53.
21. Mesenholler M, Matthews EK. A key role for the mitochondrial benzodiazepine receptor in cellular photosensitisation with δ-aminolevulinic acid. Eur J Pharmacol 2000;406:171–80.
22. Morgan J, Oseroff AR. Mitochondria-based photodynamic anti-cancer therapy. Adv Drug Deliv Rev 2001;49: 71–86.
23. Peng Q, Moan J, Nesland JM. Correlation of subcellular and intratumoral photosensitizer localization with ultrastructural features after photodynamic therapy. Ultrastruct Pathol 1996;20:109–29.
24. Susin SA, Lorenzo HK, Zamzami N, et al. Molecular characterization of mitochondrial apoptosis-inducing factor. Nature 1999;397:441–6.
25. Taketani S, Kohno H, Okuda M, Furukawa T, Tokunaga R. Induction of peripheral-type benzodiazepine receptors during differentiation of mouse erythroleukemia cells. J Biol Chem 1994;269:7527–31.
26. Taketani S, Kohno H, Furukawa T, Tokunaga R. Involvement of peripheral-type benzodiazepine receptors in the intracellular transport of heme and porphyrins. J Biochem 1995;117:875–80.
27. Wendler G, Lindemann P, Lacapere JJ, Papadopoulos V. Protoporphyrin IX binding and transport by recombinant mouse PBR. Biochem Biophys Res Commun 2003;311:847–52.
28. Rebeiz N, Arkins S, Kelley KW, Rebeiz CA. Enhancement of coproporphyrinogen III transport into isolated transformed leukocyte mitochondria by ATP. Arch Biochem Biophys 1996;333:475–81.
29. Henderson PJ, Lardy HA. Bongkrekic acid. An inhibitor of the adenine nucleotide translocase of mitochondria. J Biol Chem 1970;245:1319–26.
30. Kinnally K, Zorov DB, Antonenko YN, Snyder SH, McEnery MW, Tedeschi H. Mitochondrial benzodiazepine receptor linked to inner membrane ion channels by nanomolar actions of ligands. Proc Natl Acad Sci U S A 1993;90:1374–8.
31. Kessel D, Antolovich M, Smith KM. The role of the peripheral benzodiazepine receptor in the apoptotic response to photodynamic therapy. Photochem Photobiol 2001;74:346–9.
32. Belzacq AS, Jactot E, Vieira HLA, et al. Apoptosis induction by the photosensitizer verteporfin: identification of mitochondrial adenine nucleotide translocator as a critical target. Cancer Res 2001;61:1260–4.
33. Li LY, Luo X, Wang X. Endonuclease G is an apoptotic Dnase when released from mitochondria. Nature 2001; 412:95–9.
34. Kroemer G. The proto-oncogene Bcl-2 and its role in regulating apoptosis. Nat Med 1997;3:614–20.
35. Daugas E, Susin SA, Zamzami N, et al. Mitochondrio-nuclear translocation of AIF in apoptosis and necrosis. FASEB J 2000;14:729–39.
36. Larochette N, Decaudin D, Jacotot E, et al. Arsenite induces apoptosis via a direct effect on the mitochondrial permeability transition pore. Exp Cell Res 1999;249: 413–21.
37. Bossy-Wetzel E, Newmeyer DD, Green DR. Mitochondrial cytochrome *c* release in apoptosis occurs upstream of DEVD-specific caspase activation and independently of mitochondrial transmembrane depolarization. EMBO J 1998;17:37–49.
38. Chiu SM, Oleinick NL. Dissociation of mitochondrial depolarization from cytochrome *c* release during apoptosis induced by photodynamic therapy. Br J Cancer 2001;84:1099–106.
39. Marzo I, Brenner C, Zamzami N, et al. The permeability transition pore complex: a target for apoptosis regulation by caspases and Bcl-2-related proteins. J Exp Med 1998;187:1261–71.
40. Costantini P, Chernyak BV, Petronilli V, Bernardi P. Modulation of the mitochondrial permeability transition pore by pyridine nucleotide and dithiol oxidation at two separate sites. J Biol Chem 1996;271: 6746–51.
41. Salet C, Moreno G, Ricchelli F, Bernardi P. Singlet oxygen produced by photodynamic action causes inactivation of the mitochondrial permeability transition pore. J Biol Chem 1997;272:21938–43.
42. Godar DE. UVA1 radiation triggers two different final apoptotic pathways. J Invest Dermatol 1999;112: 3–12.

Targeting PBR by Hexaminolevulinate-Mediated Photodynamic Therapy Induces Apoptosis through Translocation of Apoptosis-Inducing Factor in Human Leukemia Cells

Ingegerd Eggen Furre, Susan Shahzidi, Zivile Luksiene, et al.

Cancer Res 2005;65:11051-11060.